



Role of graphene towards long-term stability of flexible heaters made of graphene-coated silver nanowire networks under repeated deformation

Jinyoung Hwang¹, Jungmin Lee¹, Seyoung Ryu², and Yun Sung Woo^{2,*} 

¹ School of Electronics and Information Engineering, Korea Aerospace University, Goyang-si, Gyeonggi-do 10540, Republic of Korea

² Department of Materials Science and Engineering, Dankook University, 119, Dandae-ro, Dongnam-gu, Cheonan-si, Chungnam 31116, Republic of Korea

Received: 8 August 2022

Accepted: 24 November 2022

Published online:
17 January 2023

© The Author(s), under exclusive licence to Springer Science+Business Media, LLC, part of Springer Nature 2023

ABSTRACT

The electric heaters used in wearable electronic devices require mechanical and thermal stability against deformation and flexibility. In this study, we fabricated a film heater by coating a flexible substrate with a network of silver nanowires coated with chemical-vapour-deposited graphene (denoted as GPonAgNWs) and observed the effect of the number of graphene layers on the heating performance and stability. As the number of graphene layers increased, the maximum temperature and bending cycles that the GPonAgNW network could withstand increased upon repeated bending deformation. Silver nanowire networks coated with two and four graphene layers could, respectively, withstand temperatures of 58 and 70 °C for 18,000 bending cycles at a strain of 15%, whereas a graphene-free silver nanowire network failed at 51 °C after 180 cycles. Moreover, a real-time analysis during cyclic bending deformation of the silver nanowire network coated with four-layer graphene showed a stable temperature variation within 2 °C despite the doubling of resistance for 180,000 cycles. Structural analysis and Monte Carlo simulation demonstrated that the graphene-induced reduction of the contact resistance between the two nanowires could suppress the hotspots generated at the contact, thereby providing an extended heater lifetime and stable heater performance in the GPonAgNW network. Thus, we suggest that flexible heaters made of GPonAgNW networks, exhibiting high reliability upon repeated deformation, can be used in wearable devices.

Address correspondence to E-mail: yunswoo@dankook.ac.kr

1 Introduction

Recently, electrically driven flexible heaters have attracted considerable attention because of their increasing use in a wide range of applications in vehicles, work monitoring, medicine, and individual thermal comfort controlling systems [1–10]. One of main application of flexible heaters, the heated clothing, currently uses embedded metal wires. However, these wires have several drawbacks, such as inflexibility, creation of a nonuniform heated area, and inappropriate heating power supplied by batteries. Thus, various conductive materials, such as conductive polymers, carbon nanomaterials, and metal nanowires, have been proposed to replace these metal wires used in flexible heaters [10–12].

Metal nanowires have been extensively studied as promising conductive materials for use in heaters because they are simple and inexpensive to manufacture and exhibit a lower resistance than other materials [1–3, 12–14]. Stretchable silver nanowire (AgNW) network heaters fabricated on plastic substrates and fabrics are found to operate successfully at high temperatures and high strains [2, 14]. However, the high contact resistance between contacting nanowires causes the formation of local hot spots in the AgNW network by Joule heating, accompanied by electromigration [15, 16]. Hybridization of graphene, graphene oxide, and carbon nanotubes with AgNWs has been conducted to improve the reliability and long-term stability of AgNW network heaters.

Previous studies have revealed that flexible heaters made of graphene and AgNW networks exhibit temperature uniformity and stability when subjected to mechanical deformation owing to the high electrical and thermal conductivities of graphene [17–20]. They also separately showed that the increase in resistance of the hybrid structure made of graphene and AgNW network was smaller than that of the AgNW network during cyclic bending deformation. However, both mechanical deformation and heating, especially with high strain, can increase the resistance of the AgNW network, which, in turn, affects the performance of the flexible heater. Therefore, monitoring the resistance and temperature changes during mechanical deformation will aid in understanding the role of graphene in the performance of GPonAgNW flexible heaters compared with graphene-

free AgNW network heaters; however, few studies have been conducted thus far.

In addition, despite the excellent electrical and thermal properties of chemical vapour deposition (CVD) graphene, which are superior to those of reduced graphene oxide and carbon nanotubes, its hybridization with AgNWs is limited because the wet transfer of CVD graphene onto the substrates can deteriorate the underlying AgNW films [21, 22].

In this study, a hybrid CVD-graphene-coated AgNW (GPonAgNW) network that can be used in flexible heater applications was fabricated on a plastic substrate. A number of graphene layers were coated on the AgNW network by transferring it to monolayer graphene several times using a dry transfer method. The effect of the graphene layers on the performance of a GPonAgNW network heater was investigated through real-time measurement of the temperature and resistance changes of the flexible heater during cyclic deformation. Finally, the failure behaviours of GPonAgNW and AgNW network heaters were analysed through electron microscopy and Monte Carlo simulation. In this study, we determined the role of CVD graphene and effective number of graphene layers in enhancing the performance of GPonAgNW flexible heaters, including sustainable temperature and stability. However, the number of graphene layers required for stable heater performance depends on the conductivity of the CVD graphene, resistance of the AgNW network, and strain condition of cyclic bending.

2 Experimental

2.1 Synthesis of CVD graphene and AgNW films

CVD graphene was synthesized on a 25 μm thick Cu foil (99.7% purity) using a low pressure CVD method. A mixture of hydrogen and methane gases (H_2 3 sccm/ CH_4 47 sccm) was introduced into a quartz tube furnace and heated to 1000 $^\circ\text{C}$ under a pressure of 460 mTorr, followed by the annealing of the Cu foil for 30 min in a hydrogen atmosphere. To coat the AgNWs with graphene, a dry transfer method using a thermal release tape (Graphene supermarket) was adopted. The adhesive layer of the tape was placed on the as-grown CVD graphene on the Cu foil and pressure applied to the tape using a rubber roll [23].

The Cu foil was then etched with a solution of ammonium persulfate dissolved in deionised water, which made only the graphene attached to the thermal release tape to remain. An AgNW network was formed on a polyethylene terephthalate (PET) substrate using a wet coating method. Commercially available AgNWs dispersed in distilled water at a concentration of 0.5 wt% were purchased from DUKSAN Hi-Metal Corporation. The approximate average diameter and length of the AgNWs were 40 nm and 20 μm , respectively. The AgNW solution was coated on the PET substrate using a machine-controlled Meyer-rod coating apparatus, and the coated film was dried for 3 min at 100 $^{\circ}\text{C}$ in an air circulating oven.

2.2 Fabrication of the GPonAgNW network flexible heater

The fabrication of the GPonAgNW network flexible heater, including the preparation of CVD graphene and AgNW network films used in it, is schematically shown in Fig. 1. First, the tape with CVD graphene was pressed firmly onto the AgNW network on the PET substrate, which was then heated to 90 $^{\circ}\text{C}$, at which temperature the tape lost its adhesiveness. The graphene was thereafter separated from the thermal tape and transferred onto the AgNW network on the PET substrate. As indicated in Fig. 1, multilayer CVD graphene can be coated on AgNW networks by transferring onto them the desired number of

monolayer graphene layers. Next, a copper tape electrode was attached to the two ends of the GPonAgNW film to enable voltage and current measurements. Finally, an ultraviolet (UV) curable liquid optically clear adhesive (LOCA) was placed on the GPonAgNW film to get the top cover of the PET substrate to encapsulate it. A GPonAgNW film heater manufactured using this process is shown in Fig. S1.

2.3 Characterization

Field-emission (FE) Scanning Electron Microscopy (SEM) was used to analyse the microstructures of the GPonAgNW and AgNW network films before and after their failure (Hitachi S-4800). Raman measurements of the films using a Renishaw Micro-Raman spectroscopy system were taken to determine the crystallinity and number of CVD graphene layers in the films. To obtain the Raman spectra, all films were excited with an Ar laser that had an excitation power of 120 mW at a wavelength of 514 nm and a spot size of 1 μm . Optical transmission spectra of GPonAgNW and AgNW network films were obtained using an optical spectrometer (JASCO V-780) operating in the 300–800 nm wavelength range, and their optical transmissions were observed at a wavelength of 550 nm.

2.4 Heating temperature measurements

The GPonAgNW and AgNW network heaters used in this study had a two-terminal configuration with

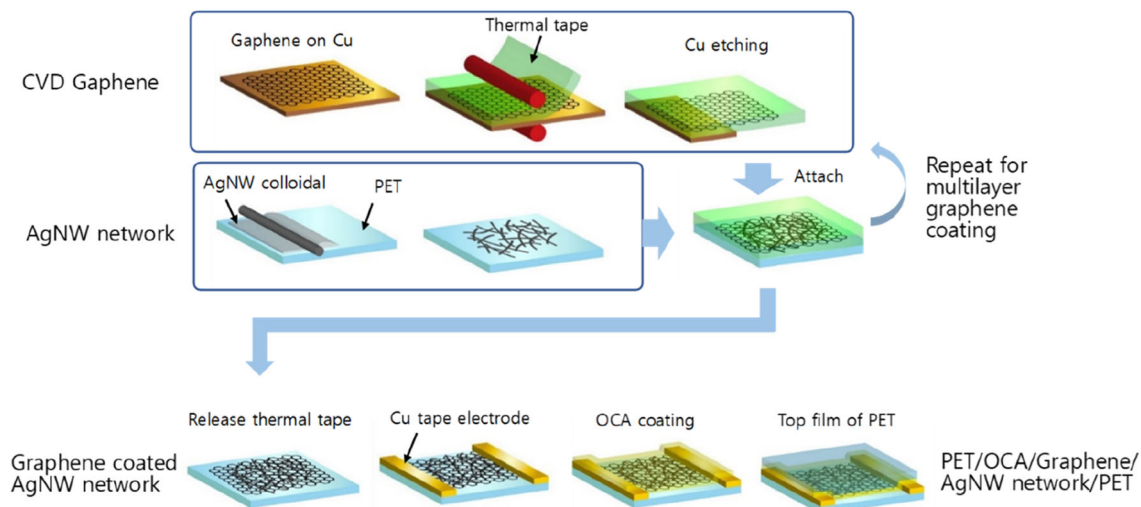


Fig. 1 Schematics showing the overall fabrication process of graphene-coated silver nanowire network flexible heater

copper electrodes at the two ends as shown in Fig. 1. A DC power supply (Keithley 2410) was used to obtain the required heating power, and the current flowing through the film heater was measured. The temperature of the film measured using a thermocouple (K-type) attached to the film surface was continuously monitored using data collection software. In addition, an infrared camera (FLK-TIS20) was used to observe the heat transfer through the film over time at an emissivity (ϵ) of 0.94, corresponding to the value of PET on top.

2.5 Cyclic bending test

The cyclic bending testing machine used in the study was custom-made. The strain applied to the film was controlled by adjusting the bending radius of the film. The cyclic bending test was performed for 18,000 cycles with a curvature radius of 2 mm, corresponding to the 15% tensile strain on the 260 μm thick film used in the experiment. To monitor the temperature changes that occurred in the GPonAgNW and AgNW network heaters during cyclic bending, a thermocouple was attached to the centre of the film surface subjected to tensile strain, while DC power was supplied to the copper electrodes to heat it. At the same time, the resistances of the GPonAgNW and AgNW network heaters for a given voltage were measured with a current meter to monitor how the resistance changed as the heater temperature changed.

2.6 Simulation

The electrical conduction characteristics of the GPonAgNW and AgNW networks were studied using a Monte Carlo simulation model, and the simulation procedure is described in detail in the Supplementary Information [24]. The GPonAgNW network was modelled using the equivalent circuit depicted in Fig. S2(d), in which the two resistors representing the AgNW network and the graphene sheet are connected in parallel. The sheet resistance of an AgNW network changes when the network is placed under a graphene layer, although its geometrical parameters remain unchanged. Previous studies on graphene and AgNW hybrid films reveal that the graphene layers covering AgNW networks can reduce the contact resistance between nanowires. A co-percolating network is formed at the highly resistive

nanowire junction, providing bypassing routes via graphene [25–28]. The reduced contact resistance between nanowires was determined by fitting the calculated sheet resistance of the GPonAgNW network to the experimental data.

3 Results and discussion

3.1 Fabrication of AgNW and GPonAgNW flexible heater

In this study, the performances of GPonAgNW and AgNW network films were studied and compared under repeated deformation to explore the possibility of using the networks in flexible heaters. Figure 2a–c shows the SEM images of the AgNW and GPonAgNW networks, respectively, in which the AgNWs are uniformly distributed to form a percolation network.

Figure 2b shows that CVD graphene was present among the AgNWs over the entire film area although it was torn at several points in the immediate vicinity of the AgNWs as indicated by the white arrows in Fig. 2c. The Raman spectrum of the graphene transferred onto SiO_2/Si substrate was obtained to observe the quality and number of graphene layers formed by transferring monolayer graphene several times. As shown in Fig. 2d, both four-layer CVD graphene obtained by transferring monolayer graphene four times and monolayer graphene exhibit excellent crystallinity with no D peaks at $\sim 1350 \text{ nm}^{-1}$. Monolayer graphene has a 2D peak at 2686 nm^{-1} with a 39.8 nm^{-1} full width at half maximum (FWHM), observed in previous studies as well [29, 30]. The position of the 2D peak in four-layer graphene is almost same as that of monolayer graphene, but its FWHM value of 47.5 nm^{-1} is larger than that of monolayer graphene, which means that adjacent graphene layers had been decoupled from each other [31]. The transmission spectra of the GPonAgNW flexible heater, composed of a top PET film, OCA, and a four-layer graphene-coated AgNW network fabricated on a PET substrate, were obtained in the region with and without graphene, respectively, as shown in Fig. S1. The optical transmittances measured at a 550 nm wavelength were 39.9% and 47.6% for the AgNW network films with and without four-layer graphene, respectively. The 7.7% difference between the two values

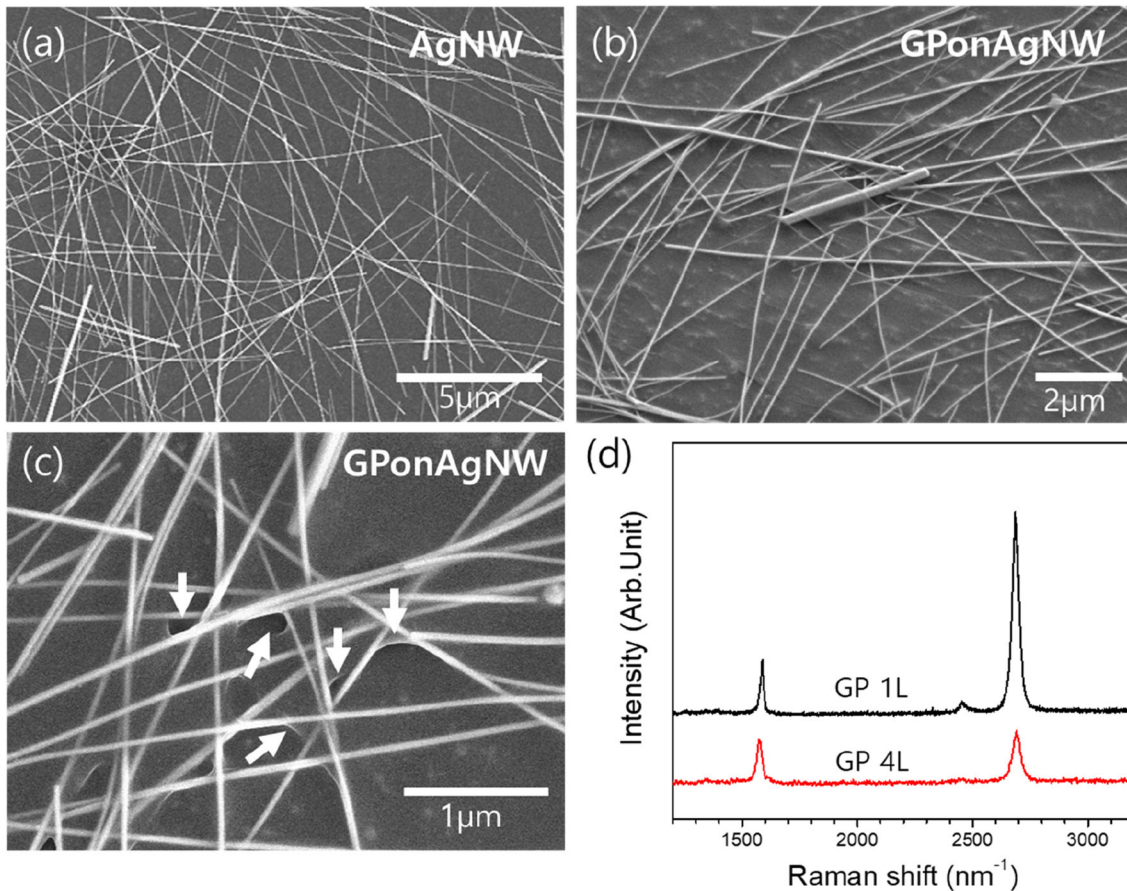


Fig. 2 SEM images of **a** AgNW and **b, c** GPonAgNW networks. White arrows in **(c)** show the graphene torn in the vicinity of the AgNWs. **d** Raman spectra of monolayer and four-layer graphene transferred on SiO₂/Si

demonstrated that four-layer graphene was successfully transferred onto the AgNW network by transferring monolayer graphene to it four times [32].

3.2 Performance comparison of AgNW and GPonAgNW network flexible heater

From Fig. 3a and b, the temperatures of the AgNW network and the two- and four-layer CVD-graphene-coated AgNW networks (GP2LonAgNW and GP4LonAgNW networks, respectively) with DC power applied can be compared. For the practical use of flexible heaters, it is necessary to determine the heating temperature as a function of resistance at a given current, because the applied voltage varies depending on the series resistance of the connected circuit. Figure 3a shows that the film temperature for a given current increases nearly linearly with the resistance when a current between 0.3 and 0.8 A is applied to the film. Here, the current level was

determined to obtain a heating temperature below the glass temperature of PET, i.e. 80 °C. For a given applied current, the temperature of the GPonAgNW network decreased as the number of coated graphene layers was increased to 0, 2, and 4. Figure 3b shows the temperature of the network as a function of the applied DC power, and it indicates the dependence of the temperature of the film on the number of graphene layers coated. The temperatures of the AgNW, GP2LonAgNW, and GP4LonAgNW network films are close to one another in the low-power region less than 2 W, independent of the number of graphene layers used. However, the temperature differences among the three films increase as the applied power is increased. The temperature of the AgNW network film is higher than that of the GP2LonAgNW network film for any given power. The GP4LonAgNW network film has the lowest temperature among the three films. Figure 3b shows that at an applied power of 7 W, the approximate temperatures

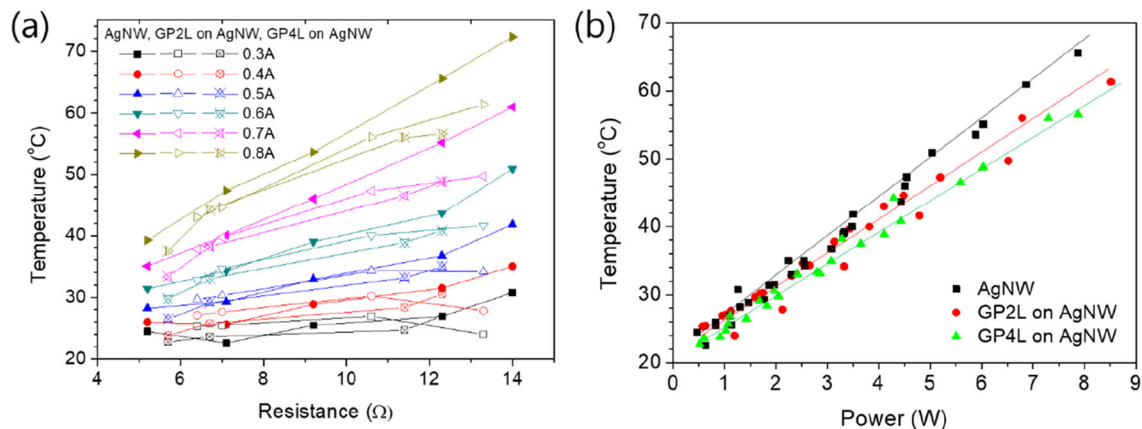


Fig. 3 Temperatures of AgNW, GP2LonAgNW and GP4LonAgNW network films plotted as functions of the **a** resistance at a fixed current between 0.3 and 0.8 A and **b** applied DC power

of AgNW, GP2LonAgNW, and GP4LonAgNW network films are 62, 56, and 53 °C, respectively.

Next, the temperature stabilities of AgNW and GPonAgNW networks were tested by subjecting them to repeated deformation. Figure 4a shows the measurement setup used for measuring the temperature at the centre of the film subjected to tensile deformation through repeated bending. Film resistances were also measured simultaneously to determine the structural changes that occurred in the AgNW and GPonAgNW networks. Figure 4b shows the temperature changes in AgNW, GP2LonAgNW, and GP4LonAgNW network films during cyclic bending up to 18,000 cycles and with an applied power of 4.3 W. As the figure shows, with the increase in the number of cycles, the temperature of the AgNW network film increases rapidly until it reaches its maximum value of 50 °C at 150 cycles and then starts to drop abruptly as the number of cycles is increased beyond 150. However, GP2LonAgNW and GP4LonAgNW network films do not show any rapid temperature changes and maintain their temperatures without any failure at 50 and 47 °C, respectively. The heating rates of AgNW, GP2LonAgNW, and GP4LonAgNW network films measured using the slope of the graph of temperature vs. time shown in Fig. 4b were compared for different applied powers. As shown in Fig. 4c, the heating rate decreases as the number of coated graphene layers is increased, which can be attributed to the increase in the heating areas of the networks caused by graphene and increased heat dissipation to the surroundings that takes place through the graphene with a high thermal conductivity. Figure 4d shows the maximum

temperatures of AgNW, GP2LonAgNW, and GP4LonAgNW network films during cyclic bending up to 18,000 cycles for different applied powers. The temperature of each of the three films was higher than that of the unstrained film indicated by the solid line in the figure, apparently because of the increase in the resistance of the deformed films. The temperature of the GP4LonAgNW network film was the highest among the temperatures of the three films. The AgNW network film had the lowest temperature. It is noticeable that the heating temperature of the three films subjected to repeated deformation was higher in the order of GP4LonAgNW, GP2LonAgNW, and AgNW network film, opposite to the order of the non-deformed by the solid line in Fig. 4b. For instance, the temperatures of the GP2LonAgNW and GP4LonAgNW network films were 59 and 74 °C, respectively, during cyclic bending and 52 and 48 °C, respectively, when unstrained at an applied power of 6.3 W.

The cyclic lifetimes of AgNW, GP2LonAgNW, and GP4LonAgNW network films are presented in Fig. 5a and b as functions of the applied power and temperature. In this experiment, cyclic bending was performed for up to 18,000 cycles; the black dotted lines in Fig. 5a and b indicate that the films did not fail during repeated bending. As shown in Fig. 5a and b, the AgNW network could be heated up to 48 °C at a power of 3.4 W without making it to fail; however, the network broke up at 180 cycles when the temperature was 51 °C and the applied power was increased to 4.3 W. By contrast, the GP2LonAgNW network could be heated up to 58 °C up to 18,000 cycles without getting it to fail. However, it

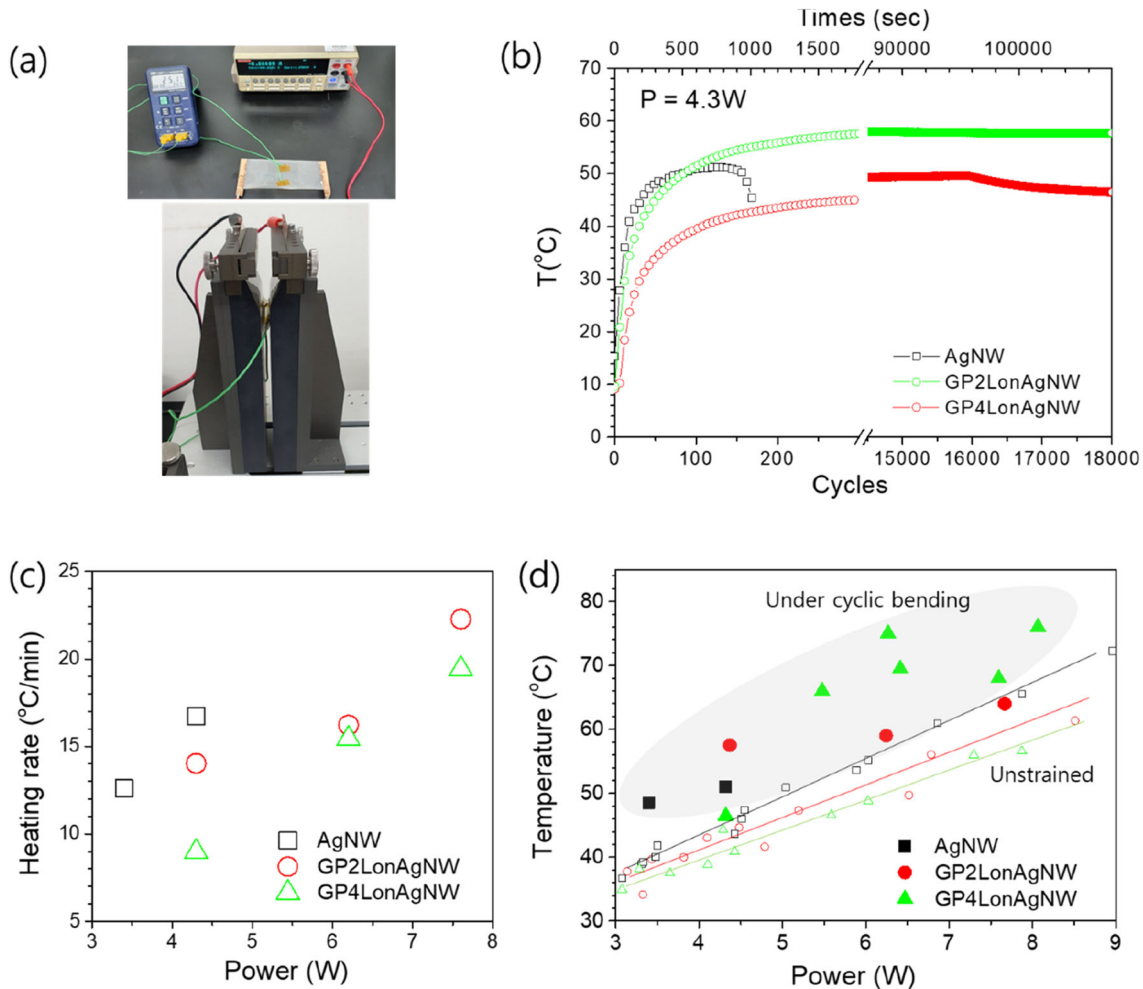


Fig. 4 **a** Experimental setup used for the in situ measurement of film temperature at the centre and resistance during cyclic bending of the film **b** Temperatures of AgNW, GP2LonAgNW and GP4LonAgNW network films during cyclic bending at a DC power of 4.3 W **c, d**) Heating rate and temperature of AgNW, GP2LonAgNW, and GP4LonAgNW network films during cyclic bending at different applied powers. The solid lines in Fig. 4d, like those in Fig. 3b, show the temperatures of the unstrained films as a function of the applied power

failed at 8015 and 3420 cycles at an applied power of 6.2 and 7.7 W, respectively. The GP4LonAgNW network could reach a maximum temperature of 70 $^{\circ}\text{C}$ without failing at an applied power of 6.4 W but started to fail as the temperature and applied power were increased further. Consequently, the maximum temperatures at which AgNW, GP2LonAgNW, and GP4LonAgNW flexible heaters can be used without any failure when subjected to long-term repeated deformation are 48, 58, and 70 $^{\circ}\text{C}$, respectively.

Next, the morphologies of the failed AgNW and GP4LonAgNW network films were observed using FE-SEM to determine the breakpoints of the two

films. As shown in Fig. 6a and b, the breakage of the AgNW network film was concentrated around a few nanowires and occurred within the contact areas of nanowires and nanowire body. However, the breakage of GP4LonAgNW network film was uniformly distributed over its entire area rather than being concentrated around a few nanowires as shown in Fig. 6c and d. Additional images showing the breakpoints in the AgNW and GPonAgNW network films are presented in Fig. S3.

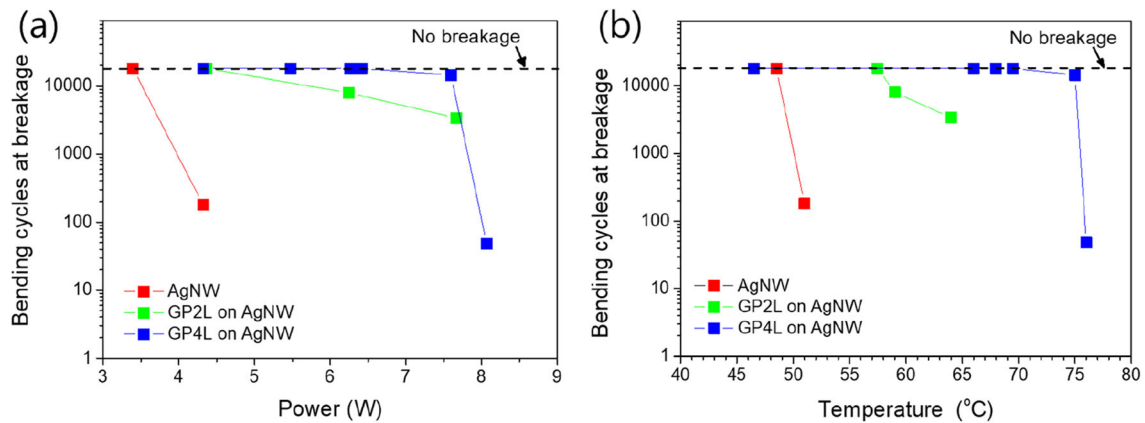


Fig. 5 Comparison of bending cycles at which AgNW, GP2LonAgNW and GP4LonAgNW samples break as a function of **a** applied DC power and **b** heating temperature

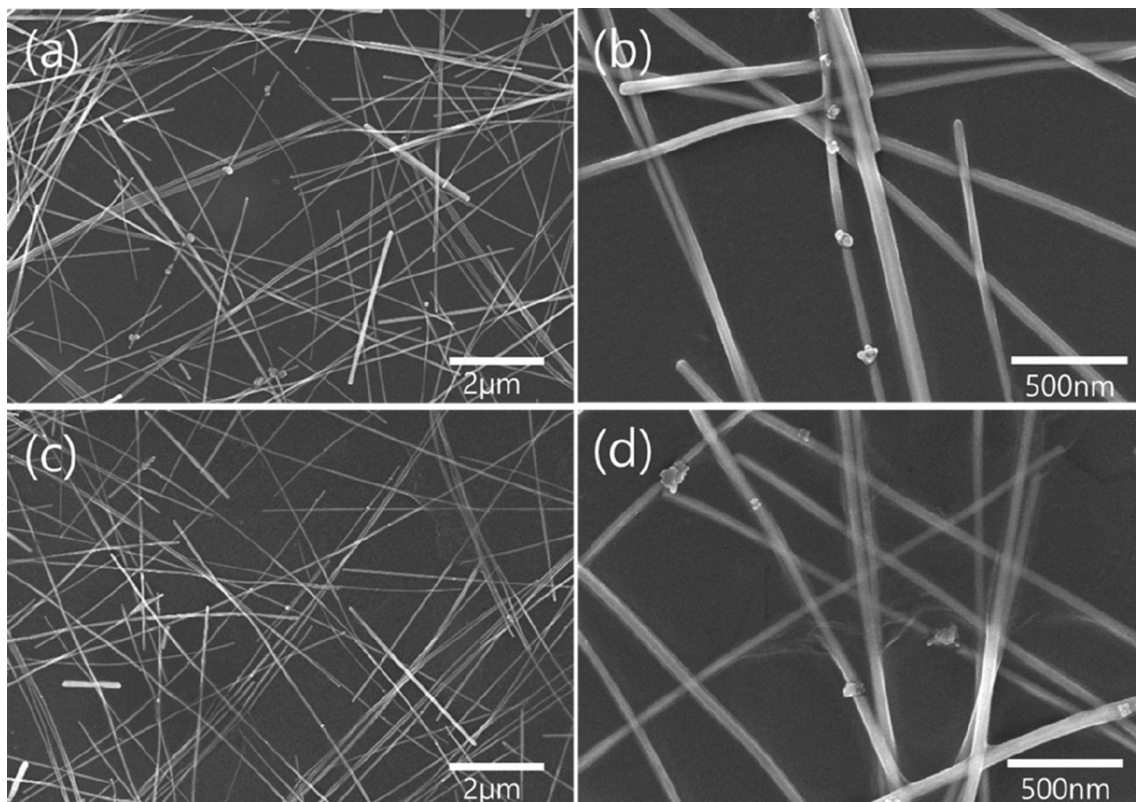


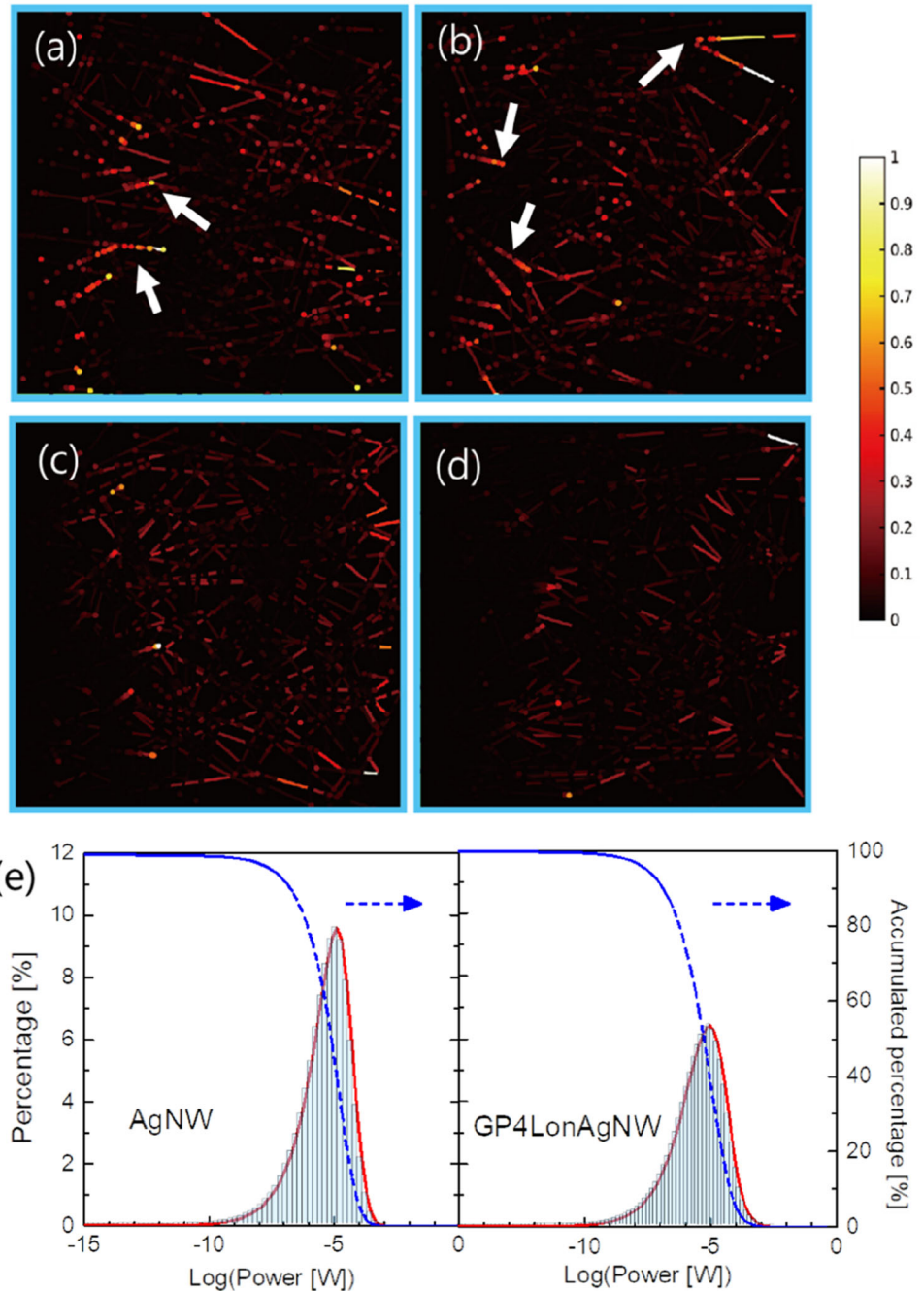
Fig. 6 **a** and **b** SEM images showing the breakpoints of AgNW network films after they have failed and **c** and **d** SEM images showing the breakpoints of GP4LonAgNW network films after they have failed

3.3 Monte Carlo simulation of AgNW and GPonAgNW network

Breakage behaviours of the AgNW and GP4LonAgNW network films were simulated using the Monte Carlo-based numerical model. Figure 7 shows the normalized electrical power distributions in the

AgNW and GP4LonAgNW networks, representing the heat dissipation in the networks. As indicated by the white arrows in Fig. 7a and b, the highest power generation is primarily concentrated along a few nanowires, which means that the temperature of the power-concentrated nanowires is higher than in other parts of the film. Consequently, the nanowires

Fig. 7 Representative instances of the normalized electrical power distribution obtained from numerical simulations: **a** and **b** AgNW and **c** and **d** GP4LonAgNW network films. White arrows in Fig. 7a and b point to the nanowires generating concentrated electrical power. **e** Histograms showing the distribution of power generated in the contact between nanowire in AgNW and GP4LonAgNW, respectively



are more susceptible to damage than the other areas. As shown in Fig. 7c and d, the GP4LonAgNW network film with low contact resistance between nanowires has a relatively uniform power distribution, indicating that nanowire breakage occurred over the entire area. Additional electrical power distributions of the AgNW and GP4LonAgNW network films are shown in Fig. S4. The change in electrical power distribution with contact resistance can be attributed to the microscopically

inhomogeneous distribution of nanowires in the percolating networks. When the contact resistance of nanowires becomes a predominant factor in determining the sheet resistance of the AgNW networks, the resistance values in each local area vary depending on the morphology of the nanowire network at the corresponding location. As a result, the current is concentrated in the low resistance region, causing some of the nanowires to generate higher power. However, as the contact resistance becomes

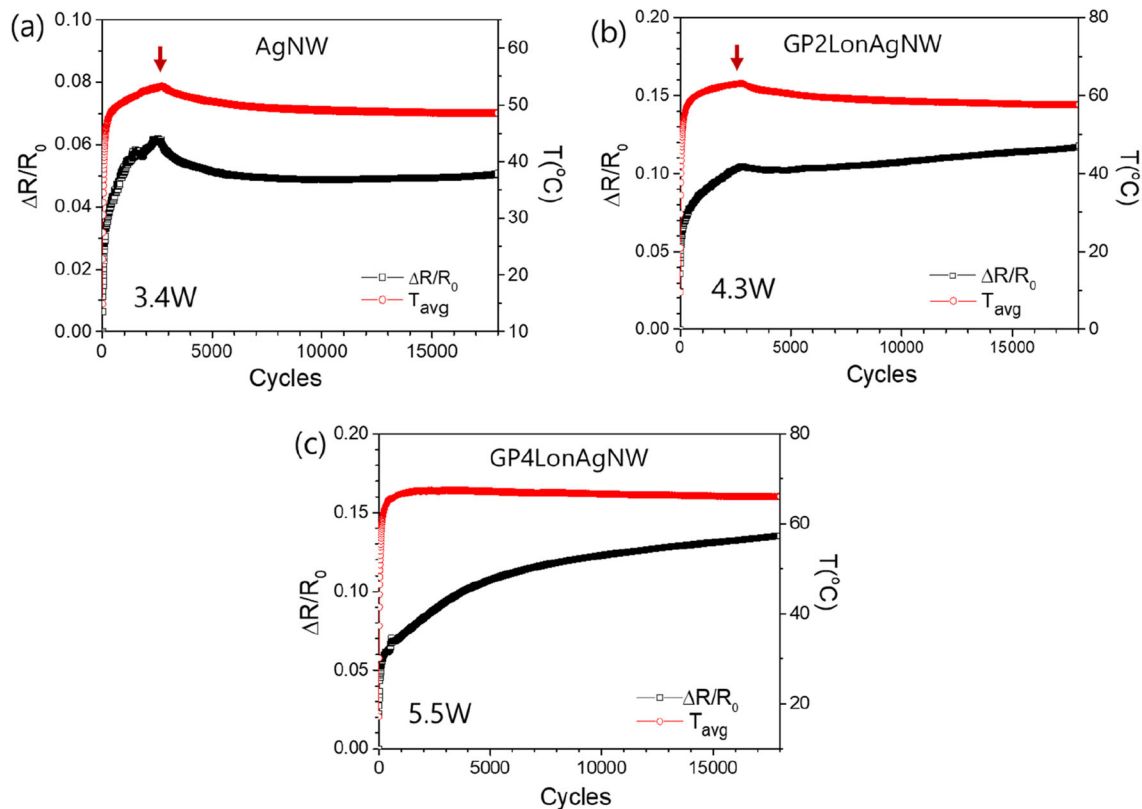


Fig. 8 Changes in the temperature (open red circle) and resistance (open black rectangular) of **a** AgNW, **b** GP2LonAgNW, and **c** GP4LonAgNW network films during cyclic bending

comparable to or less than the inherent nanowire resistance, the morphology dependency of the network resistance decreases, allowing a homogeneous current to flow through the entire network and providing a uniform power distribution. The histograms in Fig. 7e indicate the distribution of generated power at the contact between the nanowires in AgNW and GP4LonAgNW, respectively, with the majority of values falling between 10^{-10} and 10^{-3} W. Comparing the histograms of AgNW and GP4LonAgNW, AgNW has a higher proportion of nanowire contacts generating higher power than GP4LonAgNW. For instance, the percentage of contacts that generate power higher than 10^{-5} W is about 45% for AgNW, while 35% for GP4LonAgNW. Therefore, it is expected that more junctions between nanowires will be heated to higher temperatures in AgNW networks. The results are also consistent with the uniformly distributed breakpoints of nanowires in GP4LonAgNW, as observed in SEM images of Fig. 3c and d.

3.4 Real-time analysis of flexible heater performance during cyclic bending

Figure 8a–c shows the temperature and resistance changes that occurred in AgNW, GP2LonAgNW, and GP4LonAgNW network films during cyclic bending when a power of 3.4, 4.3 and 5.5 W was applied, respectively. The AgNW, GP2LonAgNW, and GP4LonAgNW network films that had not failed were selected to compare the long-term stability of each film temperature (Fig. S5). As shown in Fig. 8a, the temperature of the AgNW network film increases significantly with resistance as cyclic bending starts, reaching its maximum value of 53 °C at approximately 2500 cycles, indicated by a red arrow. Thereafter, it first decreases rapidly and then decreases gradually to reach a stable temperature of 49 °C. In Fig. 8b, the temperature and resistance of the GP2LonAgNW network film also gradually decrease after reaching their peak values at approximately 2500 cycles. However, unlike the resistance of the AgNW network film, the resistance of the GP2LonAg network film continued to increase gradually after

producing a small peak at 2500 cycles. Meanwhile, as can be seen in Fig. 8c, the temperature and resistance of the GP4LonAgNW network film do not show any peaks during cyclic bending. During cyclic bending, the temperature of the GP4LonAgNW network film remains almost same after reaching its maximum value of 67 °C, despite the significant

increase in the rate of resistance change, $\Delta R/R_0$, from 0.05 to 0.14. In all three films, the increase in the resistance at the onset of cyclic bending is due to the increase in the resistivity of metallic AgNWs at high temperatures. However, the rapid temperature drop followed by a slight peak, observed in AgNW and GP2LonAgNW network films, is probably caused by the welding of AgNW contacts due to Joule heating [33, 34]. The contact welding of AgNWs in AgNW and GP2LonAgNW could enhance the heat and current flows between nanowires, causing a decrease in the temperature and resistance of network films. Therefore, the high contact resistance between AgNWs dominates the overall current and heat flow in the AgNW and GP2LonAgNW networks. However, because four-layer graphene has a low resistance that can provide current and heat flow paths between AgNWs, contact welding of the AgNW network by Joule heating hardly decreases the resistance and temperature of the GP4LonAgNW network film. The GP4LonAgNW network film heater does not show any peaks in its resistance and temperature during cyclic bending, indicating that the increased resistance of AgNWs at high temperatures, rather than the contact resistance between AgNWs, dominates the overall current flow through the GP4LonAgNW network film. Thus, multilayer graphene of low resistance is required to obtain long-term temperature stability and extend the lifespan of a flexible heater consisting of graphene and AgNW hybrid structures.

In order to compare the heat transfer between AgNW and GP4LonAgNW network heater, the two heated shoe insoles were fabricated using an AgNW network with a resistance of 12.7 Ω and GP4LonAgNW network with a resistance of 12.3 Ω , and heated to 45 °C using a current of 0.6 A. Then, the temperature distribution of two heated shoe insole was measured at 1 min intervals using an infrared camera (Fig. S6). As a result, it was observed that the temperature of the GP4LonAgNW network is somewhat uniform in the hot region after being stabilized for 3 min, whereas the AgNW network exhibits a

nonuniform temperature distribution, adding to the temperature gradient even after the temperature has stabilized by 5 min (Fig. S6 (b) and (c)). This indicates rapid heat transfer and dissipation through the graphene layers coated on the AgNW network.

4 Conclusion

In this study, we demonstrated the performance enhancement of flexible heaters fabricated using graphene and AgNW networks by coating multiple graphene layers on AgNW networks. The operable heating temperature of the heaters during cyclic deformation increased to 76 °C at an applied power of 8.1 W when four graphene layers were coated on the AgNW network; however, the graphene-free AgNW network failed under the same conditions. The lifetime of the AgNW heater under cyclic deformation was also significantly extended by coating four layers of graphene on AgNWs, enabling a stable temperature of 70 °C without failure for more than 18,000 cycles. The results of the structural analysis conducted through SEM and Monte Carlo simulations indicated that the reduction in the contact resistance between AgNWs using a graphene layer could suppress the number of hot spots and power generated at the contact between the nanowires, thus imparting long-term stability. The GPonAgNW flexible heater showed a high-performance reliability with a temperature change within 2 °C, despite the resistance increasing by a factor of 2 during cyclic deformation over 18,000 cycles.

Acknowledgements

The present research was supported by the research fund of Dankook University in 2020.

Author contributions

All authors contributed to the study conception, design and experiment. YSW conceived the original idea of this study. JH contributed to the study design. SR and JL contributed to sample preparation and overall data collection. JH and JL contributed to the simulation and analysis. The first draft of the manuscript was written by YSW and JH and all authors

commented on previous versions of the manuscript. All authors read and approved the final manuscript.

Funding

The present research was supported by the research fund of Dankook University in 2020.

Data availability

All data generated or analysed during this study are included in this published article and its supplementary information files.

Declarations

Conflict of interest The authors declare that they have no known competing financial interests or personal relationships that could have appeared to influence the work reported in this paper.

Ethical approval This article does not contain any studies with human or animal subjects.

Informed consent It was obtained from all individual participants included in the study.

Supplementary Information: The online version contains supplementary material available at <http://doi.org/10.1007/s10854-022-09539-1>.

References

1. J. Choi, M. Byun, D. Choi, Transparent planar layer copper heaters for wearable electronics. *Appl. Surf. Sci.* **559**, 149895 (2021)
2. S. Hong, H. Lee, J. Lee, J. Kwon, S. Han, Y.D. Suh, H. Cho, J. Shin, J. Yeo, S.H. Ko, Highly stretchable and transparent metal nanowire heater for wearable electronics applications. *Adv. Mater.* **27**, 4744–4751 (2015)
3. W. Lan, Y. Chen, Z. Yang, W. Han, J. Zhou, Y. Zhang, J. Wang, G. Tang, Y. Wei, W. Dou, Ultraflexible transparent film heater made of Ag nanowire/PVA composite for rapid-response thermotherapy pads. *ACS Appl. Mater. Interfaces* **9**, 6644–6651 (2017)
4. S.-Y. Lin, T.-Y. Zhang, Q. Lu, D.-Y. Wang, Y. Yang, X.-M. Wu, T.-L. Ren, High-performance graphene-based flexible heater for wearable applications. *RSC Adv.* **7**, 27001–27006 (2017)
5. H. Sun, D. Chen, C. Ye, X. Li, D. Dai, Q. Yuan, K.W. Chee, P. Zhao, N. Jiang, C.-T. Lin, Large-area self-assembled reduced graphene oxide/electrochemically exfoliated graphene hybrid films for transparent electrothermal heaters. *Appl. Surf. Sci.* **435**, 809–814 (2018)
6. S. Bagherifard, A. Tamayol, P. Mostafalu, M. Akbari, M. Comotto, N. Annabi, M. Ghaderi, S. Sonkusale, M.R. Dokmeci, A. Khademhosseini, Dermal patch with integrated flexible heater for on demand drug delivery. *Adv. Healthc. Mater.* **5**, 175–184 (2016)
7. H. Jiang, H. Wang, G. Liu, Z. Su, J. Wu, J. Liu, X. Zhang, Y. Chen, W. Zhou, Light-weight, flexible, low-voltage electrothermal film using graphite nanoplatelets for wearable/smart electronics and deicing devices. *J. Alloys Compd.* **699**, 1049–1056 (2017)
8. Q. Liu, J. Huang, J. Zhang, Y. Hong, Y. Wan, Q. Wang, M. Gong, Z. Wu, C.F. Guo, Thermal, waterproof, breathable, and antibacterial cloth with a nanoporous structure. *ACS Appl. Mater. Interfaces* **10**, 2026–2032 (2018)
9. K. Qiu, A. Elhassan, T. Tian, X. Yin, J. Yu, Z. Li, B. Ding, Highly flexible, efficient, and sandwich-structured infrared radiation heating fabric. *ACS Appl. Mater. Interfaces* **12**, 11016–11025 (2020)
10. S. Fang, R. Wang, H. Ni, H. Liu, L. Liu, A review of flexible electric heating element and electric heating garments. *J. Ind. Text.* (2020). <https://doi.org/10.1177/1528083720968278>
11. R. Scott, The technology of electrically heated clothing. *Ergonomics* **31**, 1065–1081 (1988)
12. S. Choi, J. Park, W. Hyun, J. Kim, J. Kim, Y.B. Lee, C. Song, H.J. Hwang, J.H. Kim, T. Hyeon, Stretchable heater using ligand-exchanged silver nanowire nanocomposite for wearable articular thermotherapy. *ACS Nano* **9**, 6626–6633 (2015)
13. S. Ji, W. He, K. Wang, Y. Ran, C. Ye, Thermal response of transparent silver nanowire/PEDOT: PSS film heaters. *Small* **10**, 4951–4960 (2014)
14. T. Kim, Y.W. Kim, H.S. Lee, H. Kim, W.S. Yang, K.S. Suh, Uniformly interconnected silver-nanowire networks for transparent film heaters. *Adv. Funct. Mater.* **23**, 1250–1255 (2013)
15. H. Khaligh, L. Xu, A. Khosropour, A. Madeira, M. Romano, C. Pradère, M. Tréguer-Delapierre, L. Servant, M.A. Pope, I.A. Goldthorpe, The Joule heating problem in silver nanowire transparent electrodes. *Nanotechnology* **28**, 425703 (2017)

16. K. Maize, S.R. Das, S. Sadeque, A.M. Mohammed, A. Shakouri, D.B. Janes, M.A. Alam, Super-joule heating in graphene and silver nanowire network. *Appl. Phys. Lett.* **106**, 143104 (2015)
17. J. Kang, Y. Jang, Y. Kim, S.-H. Cho, J. Suhr, B.H. Hong, J.-B. Choi, D. Byun, An Ag-grid/graphene hybrid structure for large-scale, transparent, flexible heaters. *Nanoscale* **7**, 6567–6573 (2015)
18. P. Li, J. Ma, H. Xu, H. Zhu, Y. Liu, The role of graphene in enhancing electrical heating and mechanical performances of graphene—aligned silver nanowire hybrid transparent heaters. *Appl. Phys. Lett.* **110**, 161901 (2017)
19. J.C. Goak, T.Y. Kim, D.U. Kim, K.S. Chang, C.S. Lee, N. Lee, Stable heating performance of carbon nanotube/silver nanowire transparent heaters. *Appl. Surf. Sci.* **510**, 145445 (2020)
20. C.-L. Kim, C.-W. Jung, Y.-J. Oh, D.-E. Kim, A highly flexible transparent conductive electrode based on nanomaterials. *NPG Asia Mater.* **9**, e438–e438 (2017)
21. C.-C. Lin, D.-X. Lin, S.-H. Lin, Degradation problem in silver nanowire transparent electrodes caused by ultraviolet exposure. *Nanotechnology* **31**, 215705 (2020)
22. J. Jiu, J. Wang, T. Sugahara, S. Nagao, M. Nogi, H. Koga, K. Suganuma, M. Hara, E. Nakazawa, H. Uchida, The effect of light and humidity on the stability of silver nanowire transparent electrodes. *RSC Adv.* **5**, 27657–27664 (2015)
23. U. Lee, Y.S. Woo, Y. Han, H.R. Gutiérrez, U.J. Kim, H. Son, Facile morphological qualification of Transferred Graphene by Phase-Shifting Interferometry. *Adv. Mater.* **32**, 2002854 (2020)
24. J. Hwang, H. Sohn, S.H. Lee, Computational characterization and control of electrical conductivity of nanowire composite network under mechanical deformation. *Sci. Rep.* **8**, 1–10 (2018)
25. W.H. Chae, T. Sannicolo, J.C. Grossman, Double-sided graphene oxide encapsulated silver nanowire transparent electrode with improved chemical and electrical stability. *ACS Appl. Mater. Interfaces* **12**, 17909–17920 (2020)
26. T.T. Vo, H.-J. Lee, S.-Y. Kim, J.W. Suk, Synergistic effect of Graphene/Silver Nanowire Hybrid Fillers on highly stretchable strain sensors based on Spandex Composites. *Nanomaterials* **10**, 2063 (2020)
27. A.G. Ricciardulli, S. Yang, G.J.A. Wetzelaer, X. Feng, P.W. Blom, Hybrid silver nanowire and graphene-based solution-processed transparent electrode for organic optoelectronics. *Adv. Funct. Mater.* **28**, 1706010 (2018)
28. T. Hoon Seo, B. Kyoung Kim, G. Shin, C. Lee, M. Jong Kim, H. Kim, E.-K. Suh, Graphene-silver nanowire hybrid structure as a transparent and current spreading electrode in ultraviolet light emitting diodes. *Appl. Phys. Lett.* **103**, 051105 (2013)
29. M. Losurdo, M.M. Giangregorio, P. Capezzuto, G. Bruno, Graphene CVD growth on copper and nickel: role of hydrogen in kinetics and structure. *Phys. Chem. Chem. Phys.* **13**, 20836–20843 (2011)
30. E. Koo, S.-Y. Ju, Role of residual polymer on chemical vapor grown graphene by Raman spectroscopy. *Carbon* **86**, 318–324 (2015)
31. Y. Hao, Y. Wang, L. Wang, Z. Ni, Z. Wang, R. Wang, C.K. Koo, Z. Shen, J.T. Thong, Probing layer number and stacking order of few-layer graphene by Raman spectroscopy. *Small* **6**, 195–200 (2010)
32. R.R. Nair, P. Blake, A.N. Grigorenko, K.S. Novoselov, T.J. Booth, T. Stauber, N.M. Peres, A.K. Geim, Fine structure constant defines visual transparency of graphene. *Science* **320**, 308–1308 (2008)
33. B. Seong, I. Chae, H. Lee, V.D. Nguyen, D. Byun, Spontaneous self-welding of silver nanowire networks. *Phys. Chem. Chem. Phys.* **17**, 7629–7633 (2015)
34. T.-B. Song, Y. Chen, C.-H. Chung, Y. Yang, B. Bob, H.-S. Duan, G. Li, K.-N. Tu, Y. Huang, Y. Yang, Nanoscale joule heating and electromigration enhanced ripening of silver nanowire contacts. *ACS Nano* **8**, 2804–2811 (2014)

Publisher's Note Springer Nature remains neutral with regard to jurisdictional claims in published maps and institutional affiliations.

Springer Nature or its licensor (e.g. a society or other partner) holds exclusive rights to this article under a publishing agreement with the author(s) or other rightsholder(s); author self-archiving of the accepted manuscript version of this article is solely governed by the terms of such publishing agreement and applicable law.